Nature of the Cycloheptatrienyl–Transition Metal Bond. A Study of Electron Distribution in the Mixed-Ring Sandwich Molecules [Ti(η-C_7H_7)(η-C_5H_5)], [Nb(η-C_7H_7)(η-C_5H_5)], [Ta(η-C_7H_7)(η-C_5H_4Me)], and [Mo(η-C_7H_7)(η-C_5H_5)] by Photoelectron Spectroscopy with Variable Photon Energy

Jennifer C. Green,*,† Nikolas Kaltsoyannis,† Kong Hung Sze,† and Michael MacDonald‡

Contribution from the Inorganic Chemistry Laboratory, University of Oxford, South Parks Road, Oxford OX1 3QR, Great Britain, and SERC Daresbury Laboratory, Daresbury, Warrington WA4 4AD, Great Britain

Received August 9, 1993®

Abstract: The photoelectron spectra of [Ti(η-C_7H_7)(η-C_5H_5)], [Nb(η-C_7H_7)(η-C_5H_5)], [Ta(η-C_7H_7)(η-C_5H_4Me)], and [Mo(η-C_7H_7)(η-C_5H_5)] have been acquired with synchrotron radiation in the incident photon energy range 20–95 eV. Relative partial photoionization cross sections have been derived for the valence bands. The $1a_1$ highest occupied molecular orbital (in [Nb(η-C_7H_7)(η-C_5H_5)], [Ta(η-C_7H_7)(η-C_5H_4Me)], and [Mo(η-C_7H_7)(η-C_5H_5)]) is confirmed as almost wholly metal-localized. The principal source of metal–cycloheptatrienyl ring covalent bonding is found to be the $1e_2$ molecular orbitals. The mixed metal/ligand character of the $1e_2$ orbitals, estimated as around 60–80% metal character, indicates that neither the +1 nor the −3 formalism for the charge on the cycloheptatrienyl ring is an accurate description of the metal–ring bonding in these complexes. It is considered that three metal valence electrons are required to form the metal–cycloheptatrienyl bond.

Introduction

The cycloheptatrienyl ring is of particular interest among the aromatic carbocyclic ligands in possessing a doubly degenerate e_2 symmetry highest occupied molecular orbital (HOMO) which contains one electron. As both a +1 and a −3 formal charge therefore satisfy the Hückel $4n + 2$ rule for aromaticity, the interaction of the cycloheptatrienyl ring with a transition metal center via its e_2 level raises interesting questions of electron localization. Aside from the intrinsic theoretical interest, an understanding of the bonding between transition metals and the cycloheptatrienyl ring is of key importance in rationalizing and predicting the number and nature of ancillary ligands which the metal center can support. In a recent publication concerning the synthesis and the electronic and molecular structures of some (η-cycloheptatrienyl)(η-cyclopentadienyl) derivatives of the group V metals,[1] we addressed the nature of the (η-C_7H_7)–transition metal bond using helium discharge lamp photoelectron spectroscopy (PES) in conjunction with theoretical considerations and electrochemical, electron spin resonance (ESR), and X-ray crystallographic techniques.

In this paper we report a more extensive photoelectron (PE) spectroscopic investigation of the bonding in [M(η-C_7H_7)(η-C_5H_5)] systems, in which we have used synchrotron radiation to provide access to a wide range of incident photon energies. The information which can be obtained from the PES experiment is greatly increased when the energy of the exciting radiation is continuously tunable. In previous studies of a wide range of chemical systems,[2-9] we have demonstrated some of the problems associated with drawing conclusions from conventional discharge lamp PES and have established the variable photon energy technique as a powerful tool in electronic structure determination. The observation of features such as delayed maxima, Cooper minima, p → d, and shape reasonances in the photoionization cross sections of valence MOs has furnished a more thorough understanding of electron distribution and facilitated unequivocal assignment of PE spectra. Of particular relevance to the present work are our investigations of [M(η-C_5H_5)$_2$] (M = Fe, Ru, Os),[3] [Mn(η-C_6H_5R)$_2$] (M = Cr, R = H; M = Mo, R = Me),[7] and [U(η-C_8H_8)$_2$],[4] with which extensive comparison is made.

We have targeted four mixed sandwich molecules for investigation, [Ti(η-C_7H_7)(η-C_5H_5)], [Nb(η-C_7H_7)(η-C_5H_5)], [Ta(η-C_7H_7)(η-C_5H_4Me)], and [Mo(η-C_7H_7)(η-C_5H_5)], which between them cover 16-, 17-, and 18-electron configurations and provide examples from all three transition series. Furthermore, they sublime readily to give PE spectra with well-separated bands of metal, ligand, and mixed metal/ligand character. It was therefore expected that they would yield valuable data against which our previous conclusions could be tested.

Both theoretical and experimental methods have been employed to address the bonding in mixed sandwich molecules.[1,10-17] The

† University of Oxford.
‡ SERC Daresbury Laboratory.
® Abstract published in *Advance ACS Abstracts*, February 1, 1994.

(1) Green, J. C.; Green, M. L. H.; Kaltsoyannis, N.; Mountford, P.; Scott, P.; Simpson, S. J. *Organometallics* **1992**, *11*, 3353.
(2) Cooper, G.; Green, J. C.; Payne, M. P.; Dobson, B. R.; Hillier, I. H. *J. Am. Chem. Soc.* **1987**, *109*, 3836.
(3) Cooper, G.; Green, J. C.; Payne, M. P. *Mol. Phys.* **1988**, *63*, 1031.
(4) Brennan, J. B.; Green, J. C.; Redfern, C. M. *J. Am. Chem. Soc.* **1989**, *111*, 2373.
(5) Brennan, J. B.; Green, J. C.; Redfern, C. M.; MacDonald, M. A. *J. Chem. Soc., Dalton Trans.* **1990**, 1907.
(6) Green, J. C.; Kaltsoyannis, N.; MacDonald, M. A.; Sze, K. H. *J. Chem. Soc., Dalton Trans.* **1991**, 2371.
(7) Brennan, J. G.; Cooper, G.; Green, J. C.; Kaltsoyannis, N.; MacDonald, M. A.; Payne, M. P.; Redfern, C. M.; Sze, K. H. *Chem. Phys.* **1992**, *164*, 271.
(8) Green, J. C.; Guest, M. F.; Hillier, I. H.; Jarrett-Sprague, S. A.; Kaltsoyannis, N.; MacDonald, M. A.; Sze, K. H. *Inorg. Chem.* **1992**, *31*, 1588.
(9) Davies, C. E.; Green, J. C.; Kaltsoyannis, N.; MacDonald, M. A.; Qin, J.; Rauchfuss, T. B.; Redfern, C. M.; Stringer, G. H.; Woolhouse, M. G. *Inorg. Chem.* **1992**, *31*, 3779.
(10) Davies, C. E.; Gardiner, I. M.; Grebenik, P. D.; Green, J. C.; Green, M. L. H.; Hazel, N. J.; Mtetwa, V. S.; Prout, K. *J. Chem. Soc., Dalton Trans.* **1985**, 669.
(11) Evans, S.; Green, J. C.; Jackson, S. E.; Higginson, B. *J. Chem. Soc., Dalton Trans.* **1974**, 304.
(12) Cloke, F. G. N.; Dix, A. N.; Green, J. C.; Perutz, R. N.; Seddon, E. A. *Organometallics* **1983**, *2*, 1150.
(13) Warren, K. D. *Struct. Bonding* **1976**, *27*, 45.
(14) Clack, D. W.; Warren, K. D. *J. Organomet. Chem.* **1978**, *152*, C60.

0002-7863/94/1516-1994$04.50/0

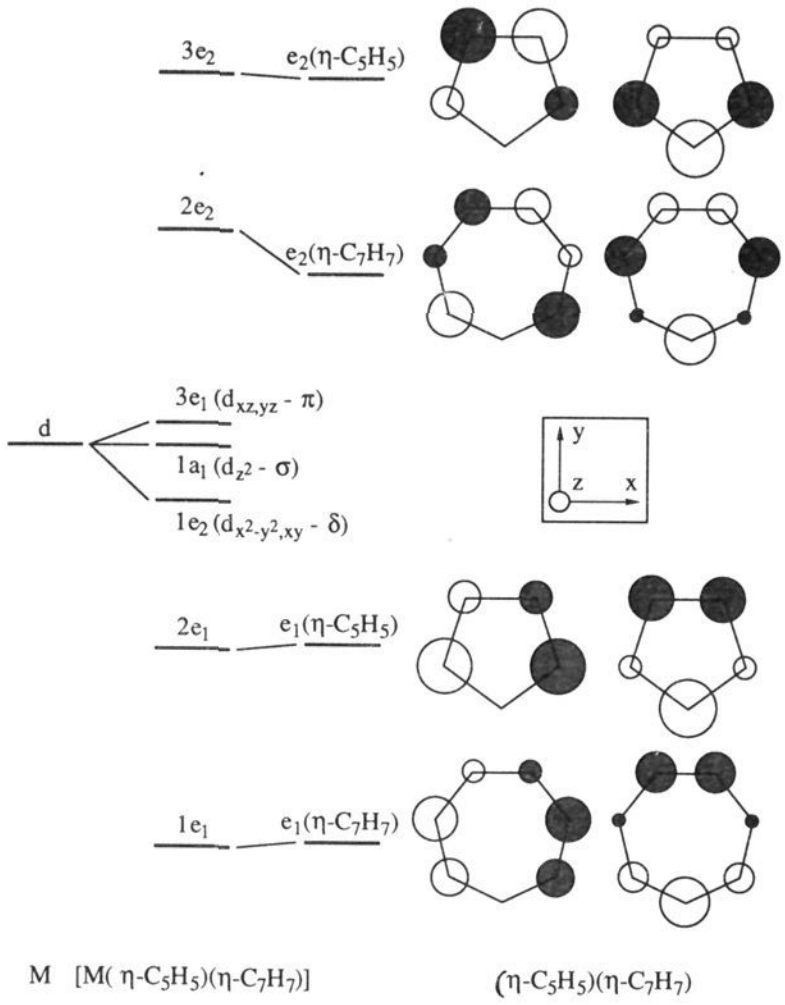

Figure 1. Qualitative molecular orbital diagram for [M(η-C_7H_7)(η-C_5H_5)], with symmetry labels appropriate to the $C_{\infty v}$ point group. Shadings indicate the phases of the carbon $2p_z$ atomic orbitals; the sizes of the circles on the C atoms reflect the relative contributions of their $2p_z$ orbitals to the MO, calculated at the extended Hückel level.

structural data obtained for [Mn(η-C_7H_7)(η-C_5H_5)] (M = Ti,[18] V,[19] Cr[16]) indicate that the rings are planar and parallel, and it may be reasonably assumed that [Nb(η-C_7H_7)(η-C_5H_5)], [Ta(η-C_7H_7)(η-C_5H_4Me)], and [Mo(η-C_7H_7)(η-C_5H_5)] have similar structures. Assuming infinite axes of rotation for the carbocyclic rings (an approximation made in many treatments[13]), an MO diagram may be constructed in the $C_{\infty v}$ point group.[11,13] Figure 1 presents such a scheme, in which only the interaction of the e symmetry pπ orbitals of the ligands with the metal is considered. In the pseudoaxial ligand field generated by the rings, the metal d-orbitals split into three sets, d_{z^2} ($1a_1$), d_{xz}, d_{yz} ($3e_1$), and $d_{x^2-y^2}$, d_{xy} ($1e_2$), which are of σ, π, and δ symmetry, respectively, with respect to the metal–ring axes. In [Ti(η-C_7H_7)(η-C_5H_5)], the $1e_2$ MO is the HOMO, while the $1a_1$ level is singly-occupied in [Nb(η-C_7H_7)(η-C_5H_5)] and [Ta(η-C_7H_7)(η-C_5H_4Me)] and is filled in the 18-electron [Mo(η-C_7H_7)(η-C_5H_5)].

The ring e MOs become progressively stabilized with increasing ring size,[1] and the energies of these levels with respect to the metal d-orbitals are such that an $e_1(\pi)$ interaction is the principal source of (η-C_5H_5)–metal bonding. However, the $e_2(\delta)$ MOs provide the more important interaction for the seven-membered ring. The cycloheptatrienyl e_1 orbitals are the main contributors to the $1e_1$ complex MOs, while the $2e_1$ levels are predominantly cyclopentadienyl in character.

Of the more metal-based MOs, the $3e_1$ MOs are antibonding while the $1a_1$ MO is largely nonbonding (the nodal cone of the d_{z^2} orbital intersects the metal-directed lobes of the C $2p_z$ orbitals of the rings close to their region of maximum electron density[12]). ESR evidence strongly supports the metal nd_{z^2} nature of the $1a_1$ MO.[1,12]

The $1e_2$ orbitals are metal→carbon back-bonding, and the cycloheptatrienyl e_2 orbital content of these complex MOs is of central importance in determining the nature of the (η-C_7H_7)–transition metal bond. If these MOs are found to be largely metal-localized, the conclusion must be that there is relatively little metal→carbon back-bonding (the (η-C_7H_7) ring is functioning more as a +1 ligand), whereas if a substantial ligand contribution is revealed, the metal–ligand δ interaction is strong (the (η-C_7H_7) ring is functioning more as a −3 ligand).

The +1 formalism for the charge on the (η-C_7H_7) ring is attractive, as it leaves the ring with six pπ electrons, isoelectronic with (η-cyclopentadienyl) and arene rings. Thus [Ti(η-C_7H_7)-(η-C_5H_5)] was considered to contain a Ti(0) (d^4) metal center.[20] Subsequent evidence, however, suggested that the unipositive formalism was misleading. An extensive series of compounds [M(η-C_7H_7)L_2X] (M = Ti, Zr) exists, where L = O, N, and P donor ligands and X = halides and alkyl groups. The typically "harder" L ligands (ethers, amines) are more tightly bound than the "softer" phosphine ligands,[10,21] suggesting that the metal center is more d^0 than d^4 in character. A similar conclusion can be drawn from the infrared stretching frequency of the CO adduct in [Nb(η-C_7H_7)(η-C_5H_4Me)CO]$^+$,[1] which at 2086 cm^{-1} is beyond the range found for cationic Nb(III) complexes of the type [Nb-(η-C_5H_5)L_3(CO)X]$^+$.[22]

The evidence from a helium discharge lamp PES study of [Ti-(η-C_7H_7)(η-C_5H_5)][10] also favored a d^0 titanium(IV) center. This is in contrast, however, to our recent results on [V(η-C_7H_7)(η-C_5H_5)], [Nb(η-C_7H_7)(η-C_5H_5)], and [Ta(η-C_7H_7)(η-C_5H_4Me)],[1] in which the $1e_2$ level was found to contain a significant contribution from both ligand and metal valence atomic orbitals (AOs), a conclusion supported by theoretical studies.[13] Following this work, we proposed that the (η-C_7H_7) ligand is best described as a 7-electron donor and a trivalent ligand and that three metal electrons are required to form the (η-C_7H_7)–transition metal bond. In doing so, however, they retain a significant degree of metal character.

The aims of the present study, therefore, were to test more fully this assertion, to quantify the relative metal and ligand contributions to the $1e_2$ MOs, and to resolve the discrepancy between the results obtained for [Ti(η-C_7H_7)(η-C_5H_5)] and the group V analogues. It was also hoped that more information would be gathered concerning the nature of the resonances proposed to be molecular shape resonances that were found in the cross sections of the valence bands of [M(η-C_5H_5)$_2$] (M = Fe, Ru, Os) and [M(η-C_6H_5R)$_2$] (M = Cr, R = H; Mo, R = Me), in addition to the p → d resonances, in particular whether their occurrence is governed by the amount of metal d-orbital character in an ionizing MO or if the symmetry of the outgoing ionization channel is more important.

Experimental Section

[Ti(η-C_7H_7)(η-C_5H_5)] was synthesized by Dr. S. E. Jackson according to the literature procedure.[23] [Nb(η-C_7H_7)(η-C_5H_5)] and [Ta(η-C_7H_7)(η-C_5H_4Me)] were synthesized by Dr. P. Scott according to the published procedure,[1] and [Mo(η-C_7H_7)(η-C_5H_5)] was synthesized by Dr. P. Scott via a route analogous to that used for [Nb(η-C_7H_7)(η-C_5H_5)].[21] All compounds were characterized by NMR and elemental analysis,[21] and their spectral purity was checked by measuring their helium discharge lamp spectra prior to running at the synchrotron radiation source.

The PE spectra of [Ti(η-C_7H_7)(η-C_5H_5)], [Nb(η-C_7H_7)(η-C_5H_5)], [Ta(η-C_7H_7)(η-C_5H_4Me)], and [Mo(η-C_7H_7)(η-C_5H_5)] were obtained using the synchrotron radiation source at the SERC's Daresbury Laboratory. A full account of our experimental method has been given,[2]

(15) Groenenboom, C. J.; Sawatsky, G.; de Liefde Meijer, H. J.; Jellinek, F. *J. Organomet. Chem.* **1974**, *76*, C4.
(16) Groenenboom, C. J.; de Liefde Meijer, H. J.; Jellinek, F. *J. Organomet. Chem.* **1974**, *69*, 235.
(17) Groenenboom, C. J.; de Liefde Meijer, H. J.; Jellinek, F.; Oskam, A. *J. Organomet. Chem.* **1975**, *97*, 73.
(18) Zeinstra, J. D.; de Boer, J. L. *J. Organomet. Chem.* **1973**, *54*, 207.
(19) Engebreston, G.; Rundle, K. E. *J. Am. Chem. Soc.* **1963**, *85*, 481.
(20) Datta, S.; Fischer, M. B.; Wreford, S. S. *J. Organomet. Chem.* **1980**, *188*, 353.
(21) Scott, P. D. Phil. Thiesis, University of Oxford, 1991.
(22) Jalon, F. A.; Otero, A.; Royo, P.; Balcazar, J. L.; Florencio, F.; Garcia-Blanco, S. *J. Chem. Soc., Dalton Trans.* **1989**, 79.
(23) van Oven, H. O.; de Liefde Meijer, H. J. *J. Organomet. Chem.* **1970**, *23*, 159.

Table 1. Incident Photon Energy Ranges Used in Acquisition of the Photoelectron Spectra of $[M(\eta\text{-}C_7H_7)(\eta\text{-}C_5H_5)]$ (M = Ti, Nb, Mo) and $[Ta(\eta\text{-}C_7H_7)(\eta\text{-}C_5H_4Me)]$

compound	incident photon energy range (eV)	compound	incident photon energy range (eV)
$[Ti(\eta\text{-}C_7H_7)(\eta\text{-}C_5H_5)]$	20–80	$[Mo(\eta\text{-}C_7H_7)(\eta\text{-}C_5H_5)]$	21–80
$[Nb(\eta\text{-}C_7H_7)(\eta\text{-}C_5H_5)]$	21–80	$[Ta(\eta\text{-}C_7H_7)(\eta\text{-}C_5H_4Me)]$	20–95

and the apparatus and its performance are described elsewhere.[24] Hence only a brief account of experimental procedures is given here.

Synchrotron radiation from the 2-GeV electron storage ring at the SERC's Daresbury Laboratory was monochromated using a toroidal grating monochromator and was used to photoionize gaseous samples in a cylindrical ionization chamber. The photoelectrons were energy analyzed using a three-element zoom lens in conjunction with a hemispherical electron energy analyzer, which was positioned at the "magic angle" so as to eliminate the effects of the PE asymmetry parameter, β, on signal intensity. Multiple-scan PE spectra were collected at each photon energy required. The decay of the storage ring beam current was corrected for by linking the scan rate with the output from a photodiode positioned to intersect the photon beam after it had passed through the ionization region. The sensitivity of the photodiode to different radiation energies was determined by measuring the np^{-1} PE spectra of Ne, Ar, and Xe. These were also used to characterize and correct for a fall off in analyzer collection efficiency at PE kinetic energies <15 eV. Photoionization cross sections for the rare gases were taken from the literature.[25,26]

Sample pressure fluctuations were corrected for by collecting a "standard" calibration spectrum before and after each data spectrum. The integrated intensities of the bands in these spectra were then used as a relative measure of the sample density in the ionization region.

All four compounds were introduced into the spectrometer inside a $^1/_4$-in. diameter copper tube sealed with a naphthalene plug. The copper tubes were surrounded by Semflex noninductively wound heating wire which was used to vaporize the samples. The required heating currents were low (<1 A). A liquid nitrogen-cooled cold finger was fitted to the spectrometer to prevent diffusion of the compound into the pumps.

Band areas were obtained by deconvoluting the spectra using asymmetric Gaussian functions. Relative partial photoionization cross sections (RPPICS) were derived from these band areas using a suite of programs initially developed by Glyn Cooper and J.C.G. and subsequently installed on the Convex C220 supercomputer at the Daresbury Laboratory. Fano profiles were obtained using a program written by Glyn Cooper.[27]

Results and Discussion

The PE spectra of $[Ti(\eta\text{-}C_7H_7)(\eta\text{-}C_5H_5)]$, $[Nb(\eta\text{-}C_7H_7)(\eta\text{-}C_5H_5)]$, $[Ta(\eta\text{-}C_7H_7)(\eta\text{-}C_5H_4Me)]$, and $[Mo(\eta\text{-}C_7H_7)(\eta\text{-}C_5H_5)]$ have been measured over the incident photon energy ranges given in Table 1. Table 2 presents ionization energy (IE) data and band assignments. Figures 2, 5, 8, and 12 present selected spectra of all four molecules. RPPICS have been derived for bands A–D (Nb, Ta, Mo) and A–C (Ti). They are given in graphical form in Figures 3–4, 6–7, 9–11, and 13; the cross sections are given in numerical form together with associated errors in the supplementary material.

1. $[Mo(\eta\text{-}C_7H_7)(\eta\text{-}C_5H_5)]$. The PE spectrum of $[Mo(\eta\text{-}C_7H_7)(\eta\text{-}C_5H_5)]$, recorded at 30 and 48 eV, is presented in Figure 2. The assignment (Table 2) is as given by previous workers.[17] Bands E, F, and G are assigned to the ring C–C and C–H σ bonding MOs, together with the most stable ring π ionizations. The large number of MOs ionizing above 11 eV makes detailed assignment impossible, and no attempt was made to derive RPPICS for bands E–G.

Below an IE of 11 eV are four bands, which are assigned to the four occupied MOs of Figure 1. Band A is assigned to the metal-based $1a_1$ HOMO, and band B, to the $1e_2$ MOs; the greater width of this band implies greater vibrational excitation in the molecular ion, reflecting the metal to carbon back-bonding character of these MOs. Bands C and D are assigned to the $2e_1$ and $1e_1$ levels, respectively. The shoulder to band C (labeled C')

Table 2. Vertical IEs and Band Assignments for $[M(\eta\text{-}C_7H_7)(\eta\text{-}C_5H_5)]$ (M = Ti, Nb, Mo) and $[Ta(\eta\text{-}C_7H_7)(\eta\text{-}C_5H_4Me)]$

compound	band	IE (eV)	ion state	related MO
$[Ti(\eta\text{-}C_7H_7)(\eta\text{-}C_5H_5)]^a$	A	6.85	$^2E_2$	$1e_2$
	B	8.74	$^2E_1$	$2e_1$
	C	9.90	$^2E_1$	$1e_1$
		>11		ligand σ and π
$[Nb(\eta\text{-}C_7H_7)(\eta\text{-}C_5H_5)]^b$	A	5.85 (5.98)	$^1A_1$	$1a_1$
	B	7.00 (7.11)	$^3E_2$	$1e_2$
	B'	7.36 (7.50)	$^1E_2$	$1e_2$
	C	8.77 (8.78)		$2e_1$
	C'	9.23 (9.13)		$2e_1$
	D	10.22 (10.4)		$1e_1$
		>11		ligand σ and π
$[Mo(\eta\text{-}C_7H_7)(\eta\text{-}C_5H_5)]^b$	A	5.70 (5.87)	$^2A_1$	$1a_1$
	B	7.38 (7.55)	$^2E_2$	$1e_2$
	C	8.86 (8.93)		$2e_1$
	C'	9.25 (9.28)		$2e_1$
	D	10.38 (10.4)		$1e_1$
		>11		ligand σ and π
$[Ta(\eta\text{-}C_7H_7)(\eta\text{-}C_5H_4Me)]^c$	A	5.47	$^1A_1$	$1a_1$
	B	6.89	$^3E_2$	$1e_2$
	B'	7.21	$^1E_2$	$1e_2$
	C	8.73		$2e_1$
	C'	9.14		$2e_1$
	D	10.19		$1e_1$
		>11		ligand σ and π

[a] IE data from ref 10. [b] IE data from a remeasurement of the He I spectra prior to running at the synchrotron radiation source. Those in parentheses are from ref 17. [c] IE data from a measurement of the He I spectrum prior to running at the synchrotron radiation source.

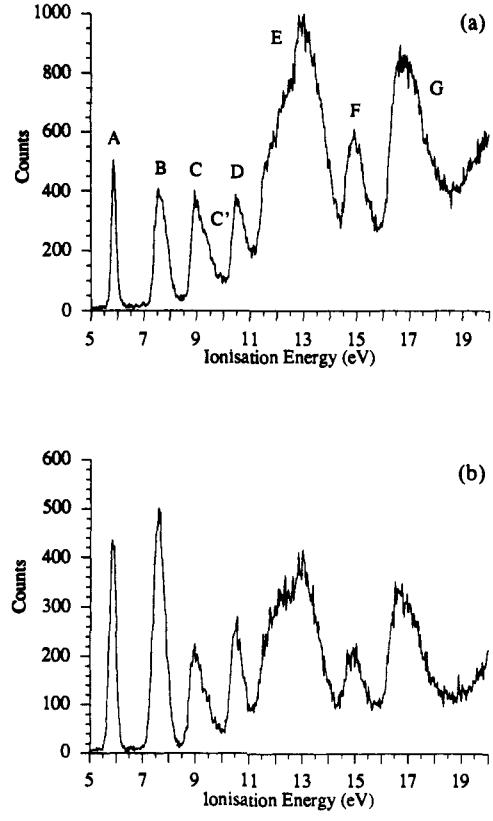

Figure 2. Photoelectron spectrum of $[Mo(\eta\text{-}C_7H_7)(\eta\text{-}C_5H_5)]$, acquired with synchrotron radiation at (a) 30 and (b) 48 eV.

(24) Potts, A. W.; Novak, I.; Quinn, G. V.; Dobson, B. R.; Hillier, I. H. *J. Phys. B* **1985**, *18*, 3177.
(25) West, J. B.; Marr, G. V. *Proc. R. Soc. London, A* **1976**, *349*, 397.
(26) West, J. B.; Morton, J. *At. Data Nucl. Data Tables* **1978**, *22*, 103.
(27) Cooper, G. D. Phil. Thesis, University of Oxford, 1987.

is more clearly visible in the HeI spectrum,[17,28] which is of slightly superior resolution to the spectra acquired with synchrotron radiation. The shape of band C is characteristic of the e_1 levels of cyclopentadienyl rings bonded to transition metals, and such structure has been observed on numerous occasions.[29-33] Its origin has been attributed to a Jahn–Teller distortion in the molecular ion,[32] although it has also been suggested that a ground state distortion of the coordinated ring,[33] or a C–H stretch,[34] may be the cause.

The spectrum of $[Mo(\eta\text{-}C_7H_7)(\eta\text{-}C_5H_5)]$ is similar to that of $[Mo(\eta\text{-}C_6H_5Me)_2]$,[7,11] with which it is isoelectronic. The major difference in the valence bands lies in the separation of bands C and D. In $[Mo(\eta\text{-}C_6H_5Me)_2]$, in which they are assigned to the e_{1u} and e_{1g} MOs resulting principally from the toluene e_{1g} levels, they lie 0.70 eV apart in IE. This splitting reflects a metal d-orbital contribution to the e_{1g} MOs, which are stabilized with respect to the e_{1u} set. However, a 1.52 eV separation is found in $[Mo(\eta\text{-}C_7H_7)(\eta\text{-}C_5H_5)]$, on account of the relative energies of the e_1 levels of the five- and seven-membered rings. The similarity in electronic structure of $[Mo(\eta\text{-}C_6H_5Me)_2]$ and $[Mo(\eta\text{-}C_7H_7)(\eta\text{-}C_5H_5)]$ will be addressed through a comparison of the RPPICS of the valence bands of $[Mo(\eta\text{-}C_7H_7)(\eta\text{-}C_5H_5)]$ with those obtained previously for $[Mo(\eta\text{-}C_6H_5Me)_2]$.[7]

The RPPICS of bands A–D of $[Mo(\eta\text{-}C_7H_7)(\eta\text{-}C_5H_5)]$ are presented in Figures 3 and 4 and will be discussed in two parts. First the predominantly metal d ionizations, the $1a_1^{-1}$ (A) and $1e_2^{-1}$ (B) bands, are discussed and second the $2e_1^{-1}$ (C) and $1e_1^{-1}$ (D) bands.

(i) **The $1a_1^{-1}$ and $1e_2^{-1}$ Bands.** The RPPICS of bands A and B are given in Figure 3a and their renormalized branching ratios (BR) (the fraction of the combined areas of bands A and B associated with each band) in Figure 3b. Below an incident photon energy of ca. 40 eV, the RPPICS of the two bands are somewhat different, with band B displaying a steep fall off from 21–40 eV (interrupted by a small shoulder at 30 eV) and band A having a minimum at 24 eV followed by a maximum at 30 eV. Subsequently both bands show maxima close to the 4p ionization potentials of free Mo ($^2P_{3/2}$ = 42 eV, $^2P_{1/2}$ = 45 eV[35]), which are attributable to resonant photoemission of 4d electrons in the vicinity of 4p → 4d giant resonant absorption, a well-established effect in both atomic and molecular photoionization.[2-9,36-41]

The 4p → 4d giant resonant absorption process for $[Mo(\eta\text{-}C_7H_7)(\eta\text{-}C_5H_5)]$ is represented by the equation

$$(4p)^6(1e_2)^4(1a_1)^2(3e_1)^0 + h\nu \rightarrow (4p)^5(1e_2)^4(1a_1)^2(3e_1)^1 \quad (1)$$

In $C_{\infty v}$ symmetry, the irreducible representations of the $4p^5$ configuration transform as $(A_1 + E_1)$, so that the states arising from the $(4p)^5(1e_2)^4(1a_1)^2(3e_1)^1$ configuration are given by the direct product

$$(A_1 + E_1) \times E_1 = {}^1E_1 + {}^1A_1 + {}^1A_2 + {}^1E_2 + {}^3E_1 + {}^3A_1 + {}^3A_2 + {}^3E_2$$

Application of the dipole selection rule and assumption of Russell–Saunders coupling give the allowed final states as $^1A_1$ and $^1E_1$. Autoionization

$$(4p)^5(1e_2)^4(1a_1)^2(3e_1)^1 \rightarrow (4p)^5(1e_2)^4(1a_1)^2(3e_1)^0 + e^- \quad (2)$$

is possible, along with the super-Coster–Kronig (SCK) decay processes

$$(4p)^5(1e_2)^4(1a_1)^2(3e_1)^1 \rightarrow \begin{cases} (4p)^6(1e_2)^3(1a_1)^2(3e_1)^0 + e^- & (3a) \\ (4p)^6(1e_2)^4(1a_1)^1(3e_1)^0 + e^- & (3b) \end{cases}$$

in which a valence electron is ionized with simultaneous relaxation of another into the hole in the 4p subshell. The final states of eqs 3a,b are identical to those produced by direct photoionization of the $1e_2$ or $1a_1$ MOs:

$$(4p)^6(1e_2)^4(1a_1)^2(3e_1)^0 + h\nu \rightarrow \begin{cases} (4p)^6(1e_2)^3(1a_1)^2(3e_1)^0 + e^- & (4a) \\ (4p)^6(1e_2)^4(1a_1)^1(3e_1)^0 + e^- & (4b) \end{cases}$$

Interchannel coupling between the corresponding final states in the resonance and direct ionization processes should lead to two overlapping Fano profiles,[42,43] resulting from absorption to the $^1A_1$ and $^1E_1$ excited states, for the RPPICS of the $1e_2^{-1}$ and $1a_1^{-1}$ bands.

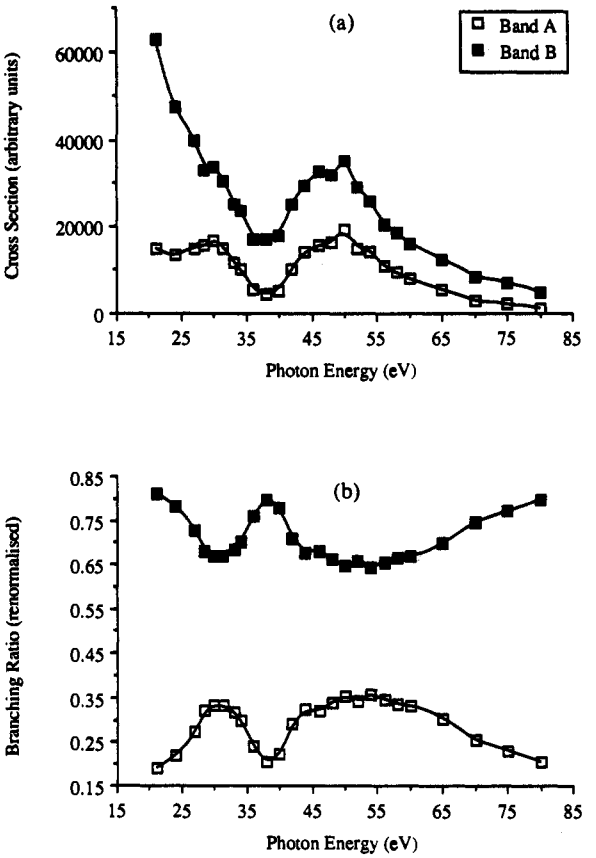

Figure 3. (a) Relative partial photoionization cross sections and (b) renormalized branching ratios of bands A and B in the photoelectron spectrum of $[Mo(\eta\text{-}C_7H_7)(\eta\text{-}C_5H_5)]$.

(28) Kaltsoyannis, N. Unpublished results, 1991.
(29) Evans, S.; Green, J. C.; Jackson, S. E. *J. Chem. Soc., Faraday Trans, 2* **1972**, *68*, 249.
(30) Lichtenberger, D. L.; Fenske, R. F. *J. Am. Chem. Soc.* **1976**, *98*, 50.
(31) Lichtenberger, D. L.; Kellogg, G. E.; Pang, L. S. K. In *Experimental Organometallic Chemistry*; Wayda, A. L., Darensbourg, M. Y., Eds.; ACS Symposium Series 357; American Chemical Society: Washington, DC, 1987; pp 265.
(32) Green, J. C. *Struct. Bonding* **1981**, *43*, 37.
(33) Calabro, D. C.; Hubbard, J. L.; Blevins, C. H.; Campbell, A. C.; Lichtenberger, D. L. *J. Am. Chem. Soc.* **1981**, *103*, 6839.
(34) Lichtenberger, D. L.; Copenhauer, A. S. *J. Chem. Phys.* **1989**, *91*, 663.
(35) Briggs, D. *Handbook of X-ray and Ultra-Violet Photoelectron Spectroscopy*; Heyden: London, 1977.
(36) Dehmer, J. L.; Starace, A. F.; Fano, U.; Sugar, J.; Cooper, J. W. *Phys. Rev. Lett.* **1971**, *26*, 1521.
(37) Bruhn, R.; Schmidt, E.; Schröder, H.; Sonntag, B. *J. Phys. B* **1982**, *15*, 2807.
(38) Bruhn, R.; Schmidt, E.; Schröder, H.; Sonntag, B. *Phys. Lett.* **1982**, *90A*, 41.
(39) Krause, M. O.; Carlson, T. A.; Fahlman, A. *Phys. Rev. A* **1984**, *30*, 1316.
(40) Kobrin, P. H.; Becker, U.; Truesdale, C. M.; Lindle, D. W.; Kerkhoff, H. G.; Shirley, D. A. *J. Electron Spectrosc. Relat. Phenom.* **1984**, *34*, 129.
(41) Richter, M.; Meyer, M.; Pahler, M.; Prescher, T.; von Raven, E.; Sonntag, B.; Wetzel, H. E. *Phys. Rev. A* **1989**, *39*, 5666.
(42) Fano, U. *Phys. Rev.* **1961**, *124*, 1866.
(43) Fano, U.; Cooper, J. W. *Phys. Rev. A* **1965**, *137*, 1364.

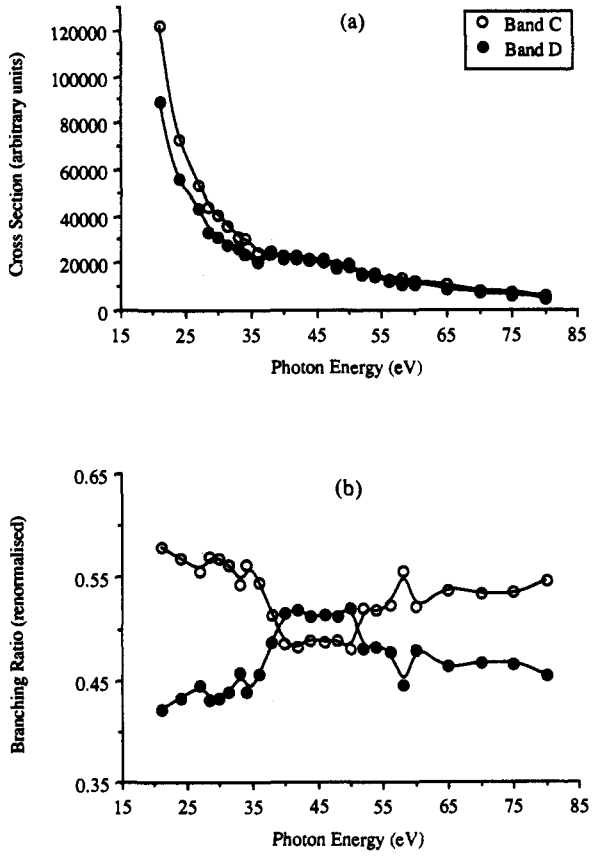

Figure 4. (a) Relative partial photoionization cross sections and (b) renormalized branching ratios of bands C and D in the photoelectron spectrum of $[Mo(\eta\text{-}C_7H_7)(\eta\text{-}C_5H_5)]$.

Fano found that, for a single resonance interacting with a single continuum channel, the cross section in the vicinity of the resonance is described by three parameters, the resonance energy E_r, the resonance width Γ, and the line profile index q. The latter measures the relative contributions of the direct and resonant ionization channels. Large q values imply large photoabsorption/SCK decay probabilities. The cross section $\sigma(E)$ as a function of incident photon energy E in the vicinity of a resonance is given by

$$\sigma(E) = \sigma_0(1 - X(E_1 - E))\frac{(q+\epsilon)^2}{(1+\epsilon^2)} \qquad (5)$$

where $\epsilon = (E - E_r)/0.5\Gamma$, σ_0 is the background cross section, X is a parameter which determines the percentage decrease in σ_0 per electronvolt, and E_1 is the lower photon energy limit of the fit. The necessity of X reflects the general decrease in MO cross sections with increasing incident photon energy (vide supra).

Fano resonance profiles were fitted to the experimentally determined RPPICS of bands A and B, using eq 5. The values of the Fano parameters obtained are given in Table 3. Satisfactory fits were obtained to two Fano profiles with identical line profile indices. Equation 5 is based on the assymption that the direct ionization process interacts with a single resonance channel. The distinct asymmetry of both RPPICS plots in this region together with the fact that two Fano profiles were required to obtain a good fit is strongly reminiscent of the data collected for $[Mo(\eta\text{-}C_6H_5Me)_2]$.[7] In that study we concluded that there is a molecular shape resonance coincident with the p → d resonance process, which between them combine to give the observed RPPICS. Strong evidence for this came from a comparison with $[Cr(\eta\text{-}C_6H_6)_2]$, in which the p → d resonance occurs at slightly higher incident photon energies (ca. 50 eV) and in which a maximum was still observed at 42 eV. That two resonance processes are occurring simultaneously means that the values of the Fano parameters are suspect.

Table 3. Fano Parameters Obtained from the RPPICS and Bands A and B in the Photoelectron Spectrum of $[Mo(\eta\text{-}C_7H_7)(\eta\text{-}C_5H_5)]$

band	q	E_r (eV)	σ_0	Γ	X	$h\nu$ range (eV)
A	1.35	43.1	6 401	8.26	0.024	38–70
		48.3		1.81		
B	0.76	41.6	17 040	10.4	0.024	38–70
		49.8		0.14		

The cross section of band A from 24–40 eV is extremely similar to the corresponding band in $[Mo(\eta\text{-}C_6H_5Me)_2]$, which is unsurprising given the almost pure Mo AO nature of the HOMO in both complexes. Of key importance, however, is the extra data point obtained for $[Mo(\eta\text{-}C_7H_7)(\eta\text{-}C_5H_5)]$ at 21 eV. That the cross section at 21 eV is higher than it is at 24 eV is strong evidence to suggest that the maximum at 30 eV is not due to the delayed maximum[44] in the cross section of the 4d AO of Mo, which was the assignment in $[Mo(\eta\text{-}C_6H_5Me)_2]$. The results on $[Mo(\eta\text{-}C_7H_7)(\eta\text{-}C_5H_5)]$ indicate that an incident photon energy of 21 eV, corresponding to a PE kinetic energy of 15.3 eV, may be taken as an upper limit to the value of the delayed maximum, in excellent agreement with the ca. 15 eV obtained from calculations on atomic Mo.[45] As there are no atomic effects which readily explain it, we therefore conclude that the maximum in band A at 30 eV is due to a molecular shape resonance.

The RPPICS of band B between 21 and 40 eV may be explained by the mixed Mo/C AO content of the $1e_2$ MOs. At low incident photon energies, the cross section of the C 2p AO contribution dominates the MO cross section, displaying the monotonic cross section fall off associated with ligand-based orbitals.[3,4,7,9] This arises from a decreased photoionization dipole matrix element as the wave function of the free electron becomes more oscillatory. The shape resonance of band A at 30 eV may be responsible for producing the shoulder to the RPPICS of the $1e_2^{-1}$ band at 30 eV, but it is not until ca. 40 eV that the metal contribution to this MO begins to reveal itself.

The branching ratio (BR) plot (Figure 3b) illustrates that both of the RPPICS maxima occur more strongly in band A than band B. The behavior of the two bands at high incident photon energies (60–80 eV) is important, in that it reveals band B to gain in intensity relative to band A. This is due to the approaching Cooper minimum[46,47] in the cross section of the 4d subshell of Mo, calculated to occur at a PE kinetic energy of 82 eV,[45] and further demonstrates the greater metal contribution to the MO giving rise to band A than band B. A similar effect was also observed in $[Mo(\eta\text{-}C_6H_5Me)_2]$.

Thus the evidence presented indicates that the $1a_1$ MO is metal-localized, with a significant metal/ligand mixing being found in the $1e_2$ levels. Comparison with the previously measured $[Mo(\eta\text{-}C_6H_5Me)_2]$ suggests that the $1a_1$ and $1e_2$ MOs of the mixed ring compound have localization properties very similar to those of $1a_{1g}$ and $1e_{2g}$ levels of the bis-arene system.

(ii) the $2e_1^{-1}$ and $1e_1^{-1}$ Bands. The RPPICS and renormalized BRs of bands C and D are presented in Figure 4a,b. Both bands display cross section behavior typical of ligand localized MOs. B and D shows a small enhancement in the region of the Mo 4p → 4d giant resonance. This may be due to a small metal d-orbital contribution to the $1e_1$ MOs or to interchannel coupling.[3] Neither the $1e_1$ nor $2e_1$ MOs has features in its RPPICS which can be identified with the shape resonances found in the more metal-localized ionizations. This is an important piece of information in determining whether MO symmetry of metal d-orbital content is the controlling influence upon the existence and magnitude of the observed shape effects. A discussion of these data is deferred

(44) Manson, S. T.; Cooper, J. W. *Phys. Rev.* **1968**, *165*, 126.
(45) Yeh, J. J.; Lindau, I. *At. Data Nucl. Data Tables* **1985**, *32*, 1.
(46) Cooper, J. W. *Phys. Rev.* **1962**, *128*, 681.
(47) Cooper, J. W. *Phys. Rev. Lett.* **1964**, *13*, 762.

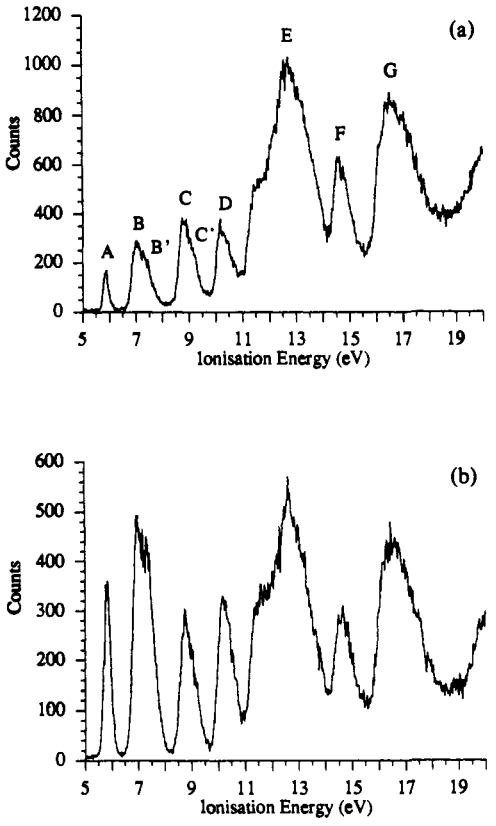

Figure 5. Photoelectron spectrum of [Nb(η-C_7H_7)(η-C_5H_5)], acquired with synchrotron radiation at (a) 30 and (b) 48 eV.

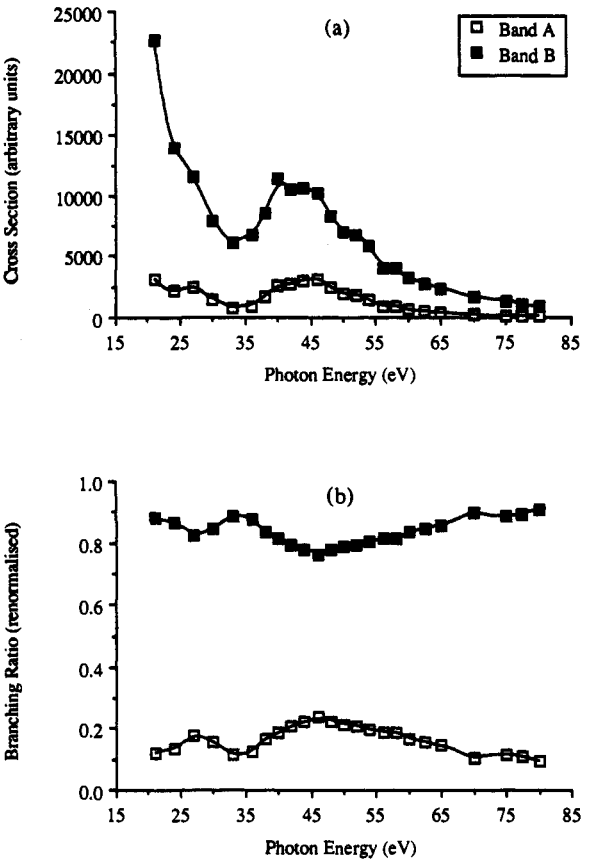

Figure 6. (a) Relative partial photoionization cross sections and (b) renormalized branching ratios of bands A and B in the photoelectron spectrum of [Nb(η-C_7H_7)(η-C_5H_5)].

until the cross section results for the other title molecules have been presented.

2. [Nb(η-C_7H_7)(η-C_5H_5)]. The PE spectrum of [Nb(η-C_7H_7)(η-C_5H_5)], recorded at 30 and 48 eV, is presented in Figure 5. The assignment is given in Table 2 and is as proposed by previous workers.[1,17] The spectrum is very similar to that of [Mo(η-C_7H_7)(η-C_5H_5)], but the relative intensity of band A is lower than that of the $1a_1^{-1}$ ionization of [Mo(η-C_7H_7)(η-C_5H_5)]. This arises from the $1a_1$ MO being singly occupied in [Nb(η-C_7H_7)(η-C_5H_5)] but doubly occupied in [Mo(η-C_7H_7)(η-C_5H_5)]. The asymmetry of band B, which is more pronounced in the He I spectrum,[1,17] is a result of an exchange interaction between the unpaired electron remaining in the $1e_2$ MOs following ionization and the electron in the $1a_1$. That of band C, which is again not well resolved in the spectra acquired with synchrotron radiation, probably arises from a Jahn–Teller distortion, as for [Mo(η-C_7H_7)(η-C_5H_5)].

The RPPICS of bands A–D are presented in Figures 6 and 7. Figure 6 gives the RPPICS of bands A and B, together with their renormalized BRs. The data are similar to those for [Mo(η-C_7H_7)(η-C_5H_5)], with both bands showing cross section enhancements in the region of the Nb 4p subshell binding energies ($^2P_{3/2}$ = 38 eV, $^2P_{1/2}$ = 40 eV[35]) and band A having another maximum at 27 eV.

The 4p → 4d giant resonant absorption process for [Nb(η-C_7H_7)(η-C_5H_5)] and subsequent SCK decay may be represented by equations similar to eqs 1–4 but reflecting the differing ground state occupancies. The half-filled a_1 shell leads to a greater number of final states, and four overlapping Fano profiles for the RPPICS of the $1e_2^{-1}$ and $1a_1^{-1}$ bands are expected via interchannel coupling between the corresponding final states in the SCK and direct ionization processes. The cross section behavior may be further complicated by the existence of a final configuration that cannot be achieved through a simple direct photoionization, namely $((4p)^6(1e_2)^3(1a_1)^0(3e_1)^1)$. It is therefore expected that the RPPICS maxima of the metal-based ionizations of [Nb(η-C_7H_7)(η-C_5H_5)] are the result of a complicated series of ionization processes, which the expected molecular shape resonance will further affect.

There are four separate features within the RPPICS enhancement of band B over the photon energy range 36–65 eV. Detailed assignment of these is not possible, but it is likely that the shape resonance occurs at the same incident photon energy as in [Mo(η-C_7H_7)(η-C_5H_5)] and therefore that it is the origin of the first maximum (at 40 eV). It is curious that this maximum is not as strong in the RPPICS of band A, unlike the two Mo complexes discussed previously. It proved impossible to fit adequately Fano functions to the RPPICS of bands A and B. Given their complicated cross section behavior—both expected and found—this is not a surprising result.

The low incident photon energy behavior of band A is analogous to that found in [Mo(η-C_7H_7)(η-C_5H_5)]. It is curious that the maximum in the shape resonance occurs 3 eV lower in [Nb(η-C_7H_7)(η-C_5H_5)] (at 27 eV), but the minimum in the RPPICS of band A at 24 eV indicates that the subsequent maximum is not due to the delayed maximum in the Nb 4d AO cross section. This is calculated to occur at a PE kinetic energy of ca. 11 eV.[45] Once again the incident photon energy of 21 eV, corresponding to a PE kinetic energy of ca. 15 eV, places an upper limit on the experimental value of the delayed maximum, but in the absence of spectra below 21 eV, no further conclusions can be drawn. The shape resonance may be mirrored in band B at 27 eV, but the effect is slight, supporting further the observation that the low photon energy shape resonance is stronger in the $1a_1^{-1}$ than the $1e_2^{-1}$ band.

The BR plot (Figure 6B) reinforces the preceding discussion and again emphasizes the mixed metal/C AO nature of the $1e_2$ MOs. The BR of the purely metal-based MO($1a_1$) decreases at high incident photon energies on account of the Cooper

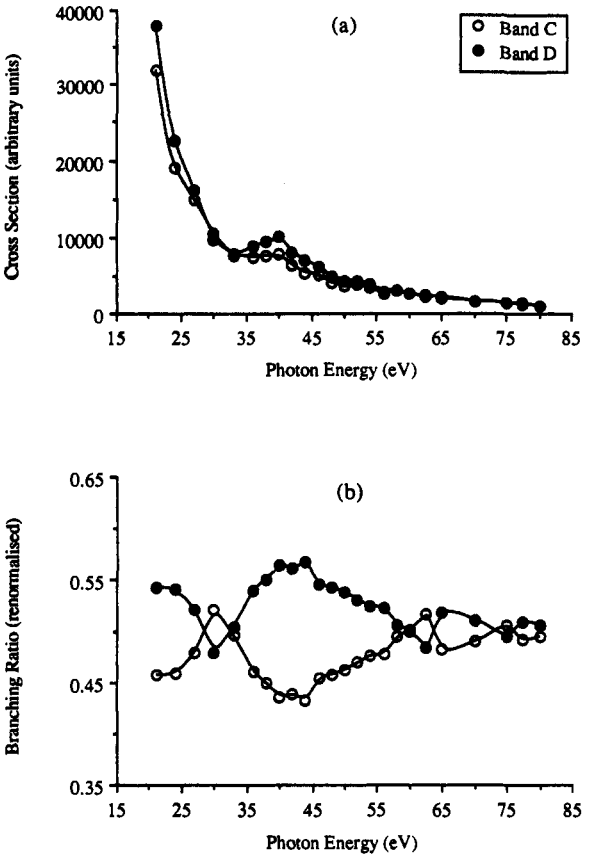

Figure 7. (a) Relative partial photoionization cross sections and (b) renormalized branching ratios of bands C and D in the photoelectron spectrum of [Nb(η-C_7H_7)(η-C_5H_5)].

minimum in the Nb 4d AO cross section (calculated to occur at a PE kinetic energy of 79 eV[45]), as was observed for the Mo complex.

In general, then, the RPPICS behaviors of the $1a_1^{-1}$ and $1e_2^{-1}$ bands of [Nb(η-C_7H_7)(η-C_5H_5)] are qualitatively similar to those of their Mo analogues; examination of Figures 3 and 6 suggests that the metal d-orbital content of the $1e_2$ MOs is approximately similar for both complexes.

Figure 7 presents the RPPICS and renormalized BRs of bands C and D. As with [Mo(η-C_7H_7)(η-C_5H_5)], the cross section variation of these two bands is somewhat different from those of bands A and B, but the slight RPPICS enhancement in band D of [Mo(η-C_7H_7)(η-C_5H_5)] in the p → d resonance region is stronger in the corresponding band of [Nb(η-C_7H_7)(η-C_5H_5)]. Band C, which displayed no metal d-orbital contribution in [Mo(η-C_7H_7)(η-C_5H_5)], has a small cross section maximum at 40 eV, although both Figures 7a,b indicate that the effect is weaker in the predominantly cyclopentadienyl-localized e_1 MOs than in their cycloheptatrienyl counterparts.

3. [Ta(η-C_7H_7)(η-C_5H_4Me)]. The recently synthesized [Ta(η-C_7H_7)(η-C_5H_4Me)][1] is the first example of a cycloheptatrienyl–Ta complex. Figure 8 presents the He I spectrum, together with that obtained using synchrotron radiation at 50 eV. It can be readily assigned by comparison with the previously reported [M(η-C_7H_7)(η-C_5H_5)] spectra. The asymmetries of bands B and C are attributed to the same causes as in [Nb(η-C_7H_7)(η-C_5H_5)], to exchange and Jahn–Teller effects, respectively.

Figure 9 gives the RPPICS of bands A and B, and Figure 10, their renormalized BRs. Both bands have cross section behavior which is different from that seen in the complexes discussed so far, with four separate maxima over the 20-95-eV incident photon energy range employed. The data for band A are particularly striking.

In the region of the p → d giant resonance (ca. 35–65 eV),

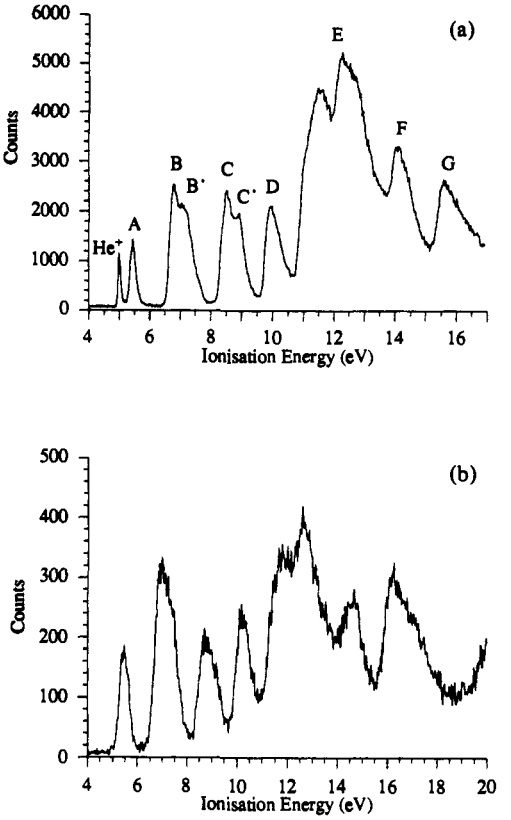

Figure 8. Photoelectron spectrum of [Ta(η-C_7H_7)(η-C_5H_4Me)], acquired (a) at 21.22 eV (He Iα) and (b) with synchrotron radiation at 50 eV.

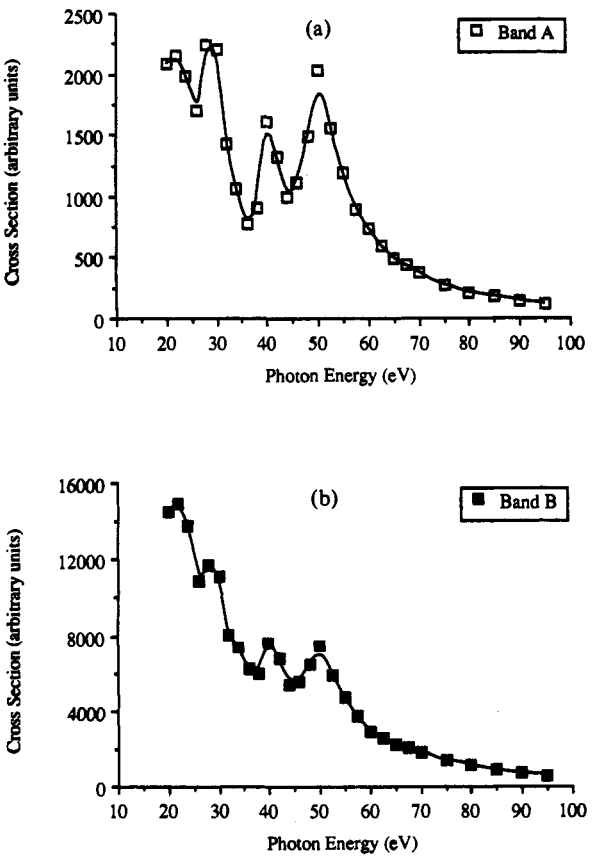

Figure 9. Relative partial photoionization cross sections of (a) band A and (b) band B in the photoelectron spectrum of [Ta(η-C_7H_7)(η-C_5H_4Me)].

there are now two distinct RPPICS maxima in both bands A and B, at 42 and 52 eV, in contrast to the second row systems discussed

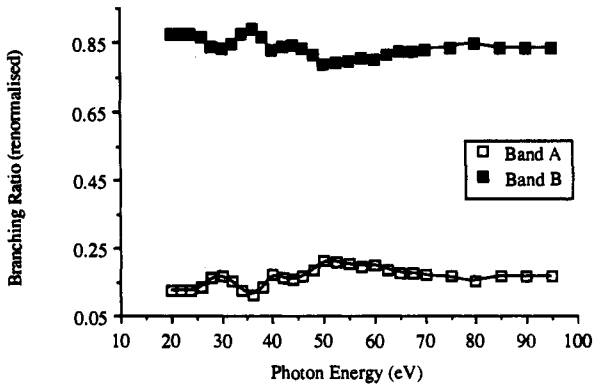

Figure 10. Renormalized branching ratios of bands A and B in the photoelectron spectrum of [Ta(η-C_7H_7)(η-C_5H_4Me)].

thus far. This is in accord with the increased splitting of the IEs of the *n*p subshell as *n* moves from 4 to 5. The $^2P_{3/2}$ and $^2P_{1/2}$ states are split by 2 eV in Nb and 3 eV in Mo, while for atomic Ta, $^2P_{3/2}$ = 38 eV and $^2P_{1/2}$ = 47 eV.[35]

The 5p → 5d giant resonant absorption process for [Ta(η-C_7H_7)(η-C_5H_4Me)] is represented by two equations

$$(5p)^6(1e_2)^4(1a_1)(3e_1)^0 + h\nu \rightarrow (5p)^5(1e_2)^4(1a_1)^2(3e^1)^0 \quad (6a)$$

$$(5p)^6(1e_2)^4(1a_1)^1(3e_1)^0 + h\nu \rightarrow (5p)^5(1e_2)^4(1a_1)^1(3e_1)^1 \quad (6b)$$

in a manner analogous to that for [Nb(η-C_7H_7)(η-C_5H_5)]. A significant difference between the two systems arises because of the increase in spin–orbit coupling effects in the third row over the second row metals, to the point at which the LS coupling scheme is no longer valid. A treatment of the p → d resonances in [$W(CO)_6$],[2] [Os(η-C_5H_5)$_2$],[3] and [U(η-C_8H_8)$_2$][4] under the j–j coupling approach led in all cases to the prediction that the first RPPICS maximum should be more intense than the second. In all cases the reverse was found in practice, as is the situation in d → f photoabsorption spectra of lanthanide and actinide elements, e.g. Th[48] and U.[49] The conclusion was that neither coupling scheme provides a valid approach, as the magnitude of exchange and spin–orbit effects are similar.[50]

Given this body of evidence, the fact that the second RPPICS maximum is again more intense than the first in both bands A and B, and the complications arising from the possibility of more than two open shells in the molecular ion (($5p^5$)($1e_2^4$)($1a_1^1$)-($1e_1^1$)) and the expected molecular shape resonance, we do not feel that a group theoretical treatment of the p → d resonance in [Ta(η-C_7H_7)(η-C_5H_4Me)] under either coupling scheme is rewarding.

The molecular potential field of [Ta(η-C_7H_7)(η-C_5H_4Me)] should not differ significantly from those of the complexes discussed so far, and a shape resonance might therefore be expected in both bands A and B at ca. 30 eV. The symmetric nature of both RPPICS enhancements suggests that, if a shape resonance is occurring, it is coincident in photon energy with one of the p → d resonance maxima.

The RPPICS of both bands A and B fit very well to two Fano profiles having identical line profile indices, one profile being used to fit each of the separate maxima at 42 and 52 eV. The values obtained are given in Table 4.

(48) Cukier, M.; Gauthe, B.; Wehnkel, C. *J. Phys.* (*Paris*) **1980**, *41*, 603.
(49) Cukier, M.; Dhez, P.; Gauthe, B.; Jaegle, P.; Wehnkel, C.; Combet-Farnoux, F. *J. Phys.* (*Paris*) **1978**, *39*, L315.
(50) Wendin, G. *Phys. Rev. Lett.* **1983**, *53*, 724.

Table 4. Fano Parameters Obtained from the RPPICS and Bands A and B in the Photoelectron Spectrum of [Ta(η-C_7H_7)(η-C_5H_4Me)]

band	q	E_r (eV)	σ_0	Γ	X	$h\nu$ range (eV)
A	1.06	38.2	1019	1.62	0.027	34–62.5
		47.6		6.93		
B	0.15	37.2	7009	4.89	0.034	36–60
		45.1		6.78		

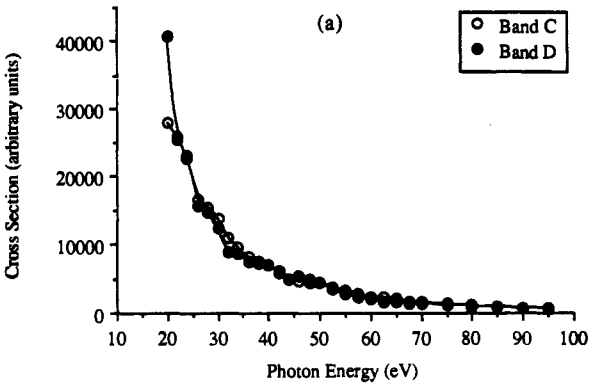

Figure 11. Relative partial photoionization cross sections of bands C and D in the photoelectron spectrum of [Ta(η-C_7H_7)(η-C_5H_4Me)].

There is a maximum in the RPPICS of both bands at 22 eV, which may be identified with the delayed maximum in the Ta 5d AO cross section. Calculations predict that this maximum should occur at about the same PE kinetic energy as that of the 4d AO of Nb (ca. 10 eV).[45] An incident photon energy of 22 eV corresponds to a PE kinetic energy of ca. 16.5 eV in band A and 15.1 eV in band B, which is somewhat higher than the predicted value. The data for [Ta(η-C_7H_7)(η-C_5H_4Me)] are the first to show a cross section maximum at these low incident photon energies, the previous RPPICS revealing only the fall off following the delayed maximum. Hence, of all of the experimental estimates of the positions of the delayed maxima, the Ta one is the most reliable.

The remaining feature in the RPPICS of bands A and B is the maximum at 28 eV. It is very likely that this is due to the molecular shape resonance seen at 27 eV in [Nb(η-C_7H_7)(η-C_5H_5)] and at 30 eV in [Mo(η-C_6H_5Me)$_2$] and [Mo(η-C_7H_7)(η-C_5H_5)]. Once again the effect is significantly greater in the $1a_1$ MO than the $1e_2$.

The BR data (Figure 10) indicate that the resonance features are stronger in the more metal-localized orbital. There is a slight gain in relative intensity of band B over band A at higher incident photon energies, but it is not as great as in the second row complexes. This is in agreement with calculation,[45] which indicates that a Cooper minimum in the cross section of the 5d AO of Ta occurs at a photon energy of ca. 190 eV, substantially higher than that of either Nb or Mo.

The RPPICS of bands C and D are given in Figure 11. Unlike the equivalent e_1^{-1} bands in [Mo(η-C_7H_7)(η-C_5H_5)] and [Nb-(η-C_7H_7)(η-C_5H_5)], the cross section behavior is typical of essentially ligand-based MOs, with no RPPICS enhancement at incident photon energies corresponding to the resonance phenomena observed in the $1a_1^{-1}$ and $1e_2^{-1}$ bands.

4. Ti(η-C_7H_7)(η-C_5H_5)]. The He I and He II spectra of [Ti-(η-C_7H_7)(η-C_5H_5)] are very similar to one another, and this lack of change in the form of the spectrum as the incident photon energy is raised from 21.22 to 40.81 eV was taken as evidence of little or no Ti 3d AO character in the $1e_2$ MOs.[10] Together with the chemical evidence discussed earlier, the discharge lamp spectra support the assertion of a Ti(IV) (d^0) metal center with the oxidation state of the cycloheptatrienyl ring being –3. In the light of substantial RPPICS enhancements of the $1e_2^{-1}$ bands in [Mo(η-C_7H_7)(η-C_5H_5)] and [Nb(η-C_7H_7)(η-C_5H_5)] in the p →

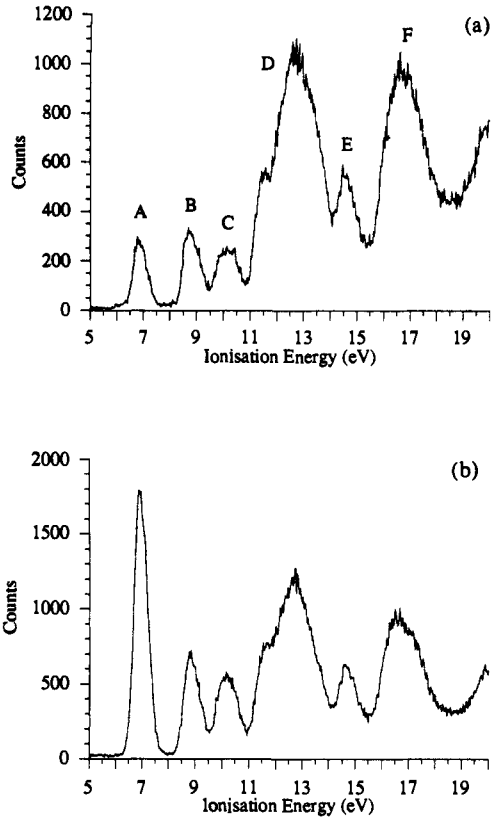

Figure 12. Photoelectron spectrum of [Ti(η-C_7H_7)(η-C_5H_5)], acquired with synchrotron radiation at (a) 33 and (b) 48 eV.

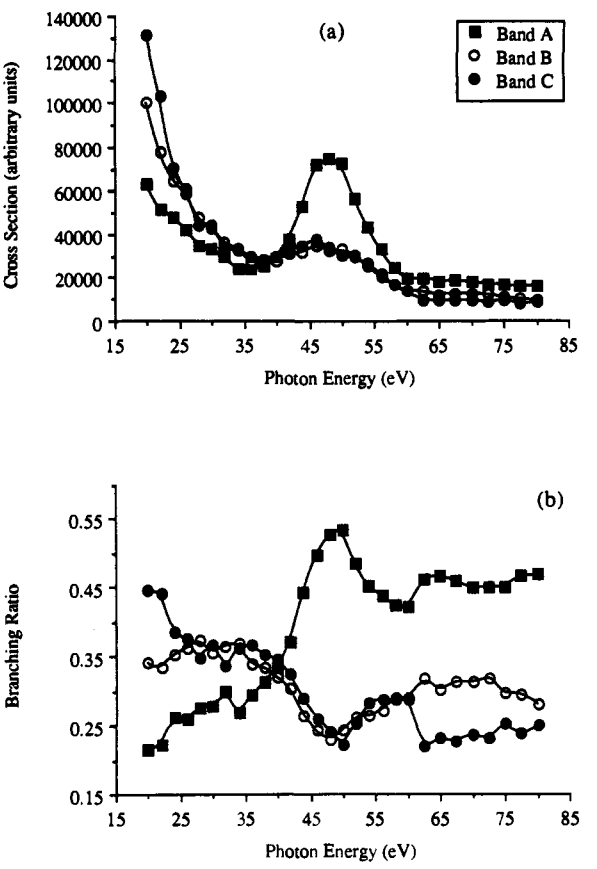

Figure 13. (a) Relative partial photoionization cross sections and (b) branching ratios of bands A–C in the photoelectron spectrum of [Ti(η-C_7H_7)(η-C_5H_5)].

d resonance regions, it was decided to investigate [Ti(η-C_7H_7)-(η-C_5H_5)] using synchrotron radiation.

The PE spectrum of [Ti(η-C_7H_7)(η-C_5H_5)], recorded at 33 and 48 eV, is shown in Figure 12. [Ti(η-C_7H_7)(η-C_5H_5)] is a 16-electron complex, and the HOMO is the $1e_2$ MO. Consequently only three bands are observed below an IE of ca. 11 eV. The change in the form of the spectrum as the incident photon energy is raised to 48 eV—just above the energy of the He IIα line—is quite dramatic, with the $1e_2^{-1}$ band (band A) undergoing a substantial increase in relative intensity. This is illustrated in Figure 13, which presents the RPPICS and BRs of bands A, B, and C. It can be seen that it is only as the incident photon energy is increased above 42 eV that the p → d resonance takes effect, providing an elegant example of the advantages of access to a continuously tunable light source.

The 3p subshell of atomic Ti ionizes at 38 ($^2P_{3/2}$) and 39 ($^2P_{1/2}$) eV.[35] Group theoretical consideration of possible absorption and decay processes along the lines of eqs 1–4 leads to the prediction of four overlapping Fano profiles for the RPPICS of the $1e_2^{-1}$ band.

The shape of the RPPICS enhancement of band A between 38 and 60 eV is unlike any seen in the other [M(η-C_7H_7)(η-C_5H_5)] molecules. It is very symmetric, and if there is a shape resonance occurring, it is obscured by the p → d resonance. It proved impossible to obtain a Fano fit to the RPPICS of band A in this region. This non-Fano enhancement may be caused by a coincident shape resonance or may reflect the presence of four possible intermediate states in the p → d giant resonant absorption process. A qualitative inspection of Figure 13a, however, indicates that the p → d resonant enhancement of the $1e_2^{-1}$ band is large—indeed its cross section is highest in the p → d resonance region. This suggests that the −3 formalism for the charge of the cycloheptatrienyl ring is not a good way of describing the cycloheptatrienyl–Ti bonding in this complex, as it implies a ligand-localized $1e_2$ MO.

There is no feature in the RPPICS of band A which correlates with the shape resonance seen in the cross sections of the $1a_1^{-1}$ and some of the $1e_2^{-1}$ bands of [M(η-C_7H_7)(η-C_5H_5)] at photon energies between 27 and 30 eV. Once more, the absence of a $1a_1^{-1}$ ionization makes it difficult to draw any conclusions from this observation, in that what was quite a strong feature in the $1e_2^{-1}$ band of [Ta(η-C_7H_7)(η-C_5H_4Me)] was not observed in [Nb-(η-C_7H_7)(η-C_5H_5)]. Similarly there is no low photon energy cross section feature which equates with a delayed maximum. For atomic titanium, the delayed maximum in the 3d orbital cross section is calculated to occur at a PE kinetic energy of ca. 23 eV,[45] which would place it at an incident photon energy of ca. 30 eV for band A.

The RPPICs of bands B and C are very similar to one another, with both displaying a significant enhancement in the p → d resonance region. As the BR plot (Figure 13b) shows, it is only in the high incident photon energy region (>60 eV) that the behavior of bands B and C differ. This is almost certainly an artefact of the curve fitting, as above 60 eV a higher analyzer pass energy is employed, resulting in poorer spectral resolution. It is therefore unlikely that the gain of band B over band C at higher photon energies is a real effect.

Estimates of Covalency. Such extensive data on a closed related series of molecules prompted us to examine whether we were able to obtain a quantitative estimate of the d-orbital character of the $1e_2$ orbital from the cross section data. Visually the behavior of the RPPICS of the $1e_2$ orbitals is intermediate between that of the metal-localized a_1 RPPICS and those of the ligand-based e_1 orbitals. There are three photon energy regions in which metal d and ligand 2p cross sections differ. At low photon energies, the ligand cross sections decay rapidly above the threshold whereas metal d cross sections can exhibit delayed maxima. Over the np → nd resonance region, the metal cross sections show resonant enhancement, whereas such enhancement is only present weakly in ligand bands as a result of interchannel coupling. At high photon energies, 4d and 5d orbitals can show Copper minima in

Table 5. Estimates of the Percentage of Metal Character in the e_2 Orbitals and the Significance of the Fit

compound	k	RSq(7)	R	α ($\alpha/\bar{b}$)	β	γ	RSq(11)	%M
[Mo(η-C_7H_7)(η-C_5H_5)]	0.63	0.923	0.986	2020 (0.078)	0.689	0.352	0.976	66
[Nb(η-C_7H_7)(η-C_5H_5)]	0.63	0.983	0.997	611 (0.087)	0.606	0.378	0.994	62
[Ta(η-C_7H_7)(η-C_5H_4Me)]	0.74	0.925	0.979	269 (0.045)	0.928	0.215	0.966	82

their cross sections, a consequence of their radial nodes. That we have identified such comparative atomic behavior in the cross sections studied here suggested that a fit to the RPPICS of the $1e_2^{-1}$ bands of the Mo, Nb, and Ta compounds by a linear combination of the RPPICS of the $1a_1^{-1}$ and $1e_1^{-1}$ bands may be possible. The presence of molecular effects, such as shape resonances, may well invalidate such an attempt, but in the molecules studied here, the strength of the shape resonance appears to correlate with the perceived d-orbital content of a MO.

Accordingly, we assumed that the $1a_1^{-1}$ and $1e_1^{-1}$ RPPICS represented ideal metal d and ligand 2p behavior, respectively, and used a least squares technique to estimate the percentage of metal character in the $1e_2$ MO. The cross sections of the $1a_1$ orbitals were multiplied by 2 in the case of the Mo compound, and 4 in the case of the Nb and Ta compounds, to give a data set a_i, which compensated for the lower occupancy of these orbitals. The RPPICS for the $1e_2$ and $1e_1$ orbitals, bands B, b_i, and D, d_i, respectively, were assumed to be related to a_i by the expression

$$b_i = ka_i + (1 - k)d_i \tag{7}$$

and a best, least squares estimate of k obtained from the expression

$$k = \frac{\sum_i (a_i - d_i)(b_i - d_i)}{\sum_i (a_i - d_i)^2} \tag{8}$$

A function g_i was defined as the residual difference between the experimental data b_i and the least squares fit:

$$g_i = b_i - ka_i - (1 - k)d_i \tag{9}$$

The quality of the fit was estimated by calculating RSq where

$$\mathrm{RSq} = 1 - \frac{\sum_i g_i^2}{\sum_i (b_i - \bar{b})^2} \tag{10}$$

The correlation between b_i and $(ka_i + (1 - k)d_i)$ was estimated by drawing the best straight line between the two sets of data points and calculating the correlation coefficient R. Values obtained are given in Table 5.

The best fit linear combination is compared with the RPPICS of the $1e_2^{-1}$ bands, and the residual difference, g_i, is plotted in Figure 14. The $1e_2$ orbitals of the second transition series compounds are estimated to have very similar d-orbital contents of 63%, while that estimated for the third row element Ta is somewhat higher at 74%. The residual is largest at low photon energy values, as might be expected as this region is where the assumptions of the Gelius model are least valid.

A more flexible expression (eq 11) was used to fit the $1e_2^{-1}$ cross sections, where a constant term, α, was included and the amounts of ligand and metal contribution were unrelated, i.e.

$$b_i = \alpha + \beta a_i + \gamma d_i \tag{11}$$

The percentage of metal character was calculated from $100\beta/(\beta + \gamma)$. Values obtained are given in Table 5. Not expectedly the RSq values improved; however, the constants found were small compared to the average value of b, $\bar{b}$, and the relative proportions of metal and ligand contribution were within 10% of those obtained using the simpler method. All results are given in Table 5.

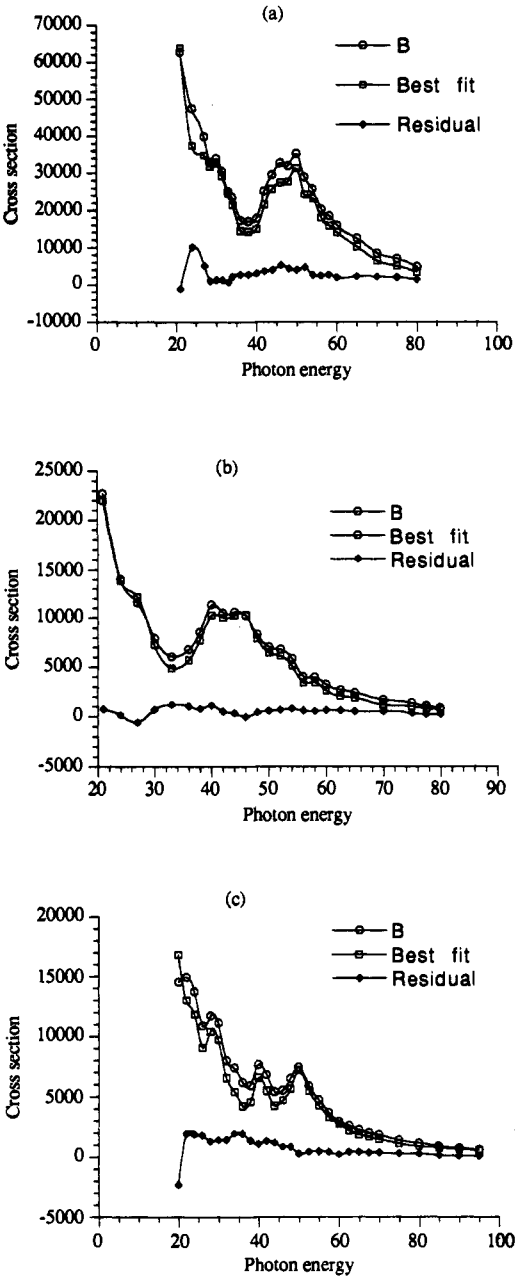

Figure 14. Comparison of the RPPICS of bands B and the best linear combination of the RPPICS of bands A and D for (a) [Mo(η-C_7H_7)-(η-C_5H_5], (b) [Nb(η-C_7H_7)(η-C_5H_5)], and (c) [Ta(η-C_7H_7)(η-C_5H_4-Me)]; the residual, g_i, is also plotted in each case.

In conclusion, the Gelius model gives a reasonably good account of the $1e_2^{-1}$ cross section in terms of the $1a_1^{-1}$ and $1e_1^{-1}$ cross sections, though it provides an underestimate which can be readily accounted for by the overlap terms at these low photon energies. It provides a way of obtaining an empirical estimate of metal character in the $1e_2$ orbital and suggests that for Mo and Nb the metal contribution is between 60 and 70%, whereas for Ta it is probably between 70 and 80%.

Summary and Conclusions

In all four molecules studied, substantial RPPICS enhancements are observed in bands corresponding to ionization from MOs with significant metal d-orbital character in the region of the *n*p subshell binding energies. This *n*p → *n*d giant resonant absorption is greatest for the $1a_1^{-1}$ bands, which are due to metal-localized MOs. It is not valid to compare directly the magnitudes of resonance phenomena between complexes containing different metals, but as all of the compounds bar [Ti(η-C_7H_7)(η-C_5H_5)] have their own "internal standard" (the $1a_1^{-1}$ band), it is possible to obtain a measure of the degree of metal d-orbital involvement in the other valence MOs. Strong evidence is found for substantial metal d-orbital involvement with the $1e_2$ levels in [Mo(η-C_7H_7)(η-C_5H_5)], [Nb(η-C_7H_7)(η-C_5H_5)], and [Ta(η-C_7H_7)(η-C_5H_4Me)]. Quantitative estimates of this effect suggest 63% metal character for the second transition series compounds and 74% for the Ta compound.

This is also the conclusion for the $1e_2$ MOs of [Ti(η-C_7H_7)(η-C_5H_5)], even without a $1a_1^{-1}$ band for reference. The very strong RPPICS enhancement that occurs at incident photon energies just above the He IIα line resolves the discrepancy between the discharge lamp spectra of [Ti(η-C_7H_7)(η-C_5H_5)] and the group V analogues and highlights the benefits of synchrotron radiation in the PES experiment. In contrast, the e_1 bands show very little metal character.

In our study of [Mo(η-$C_6H_5Me)_2$],[7] we analyzed the observed shape resonances in terms of the symmetry of the outgoing ionization channel and the amount of metal d-orbital character to the ionizing MO. This proved inconclusive, however, in that the shape resonances were found to occur only in the bands corresponding to ionization of g symmetry MOs (ionizing into u-type continuum channels), which of course are the only ones to exhibit metal d-orbital character. The data presented here for the mixed ring compounds suggest that it is metal d-orbital content which is the factor governing the magnitude and occurrence of these resonances, as the g/u symmetry notation is not defined for [M(η-C_7H_7)(η-C_5H_5)] and the shape resonances occur only in bands with metal d-orbital contributions.

The maxima in the $1a_1^{-1}$ RPPICS of [Mo(η-C_7H_7)(η-C_5H_5)], [Nb(η-C_7H_7)(η-C_5H_5)], and [Ta(η-C_7H_7)(η-C_5H_4Me)] at 27–30 eV are mirrored to some extent in the RPPICS of the mixed metal/ligand $1e_2^{-1}$ band, being visible in [Mo(η-C_7H_7)(η-C_5H_5)] and [Ta(η-C_7H_7)(η-C_5H_4Me)] but not in [Nb(η-C_7H_7)(η-C_5H_5)] (or [Ti(η-C_7H_7)(η-C_5H_5)]). As was noted for [Mo(η-$C_6H_5Me)_2$], however, the C 2p AO contribution to the RPPICS of the $1e_2^{-1}$ bands at these low incident photon energies may well be obscuring the effect.

There is clear evidence to suggest that the shape resonance seen in the $1a_{1g}^{-1}$ and $1e_{2g}^{-1}$ bands of [Mo(η-$C_6H_5Me)_2$] at ca. 42 eV also occurs in the equivalent bands of [Mo(η-C_7H_7)(η-C_5H_5)] and [Nb(η-C_7H_7)(η-C_5H_5)]. That there is no such feature in the cross section of the $1e_1^{-1}$ band of either molecule is evidence that this resonance is also primarily metal d-orbital content controlled, in that the $1e_{1g}^{-1}$ band of [Mo(η-$C_6H_5Me)_2$], which mirrors the shape resonance in the $1a_{1g}^{-1}$ and $1e^{2g-1}$ bands, is found to have significant metal d AO character, unlike the e_1^{-1} bands of the mixed ring species. This resonance is not seen in [Ta(η-C_7H_7)(η-C_5H_4Me)] or [Ti(η-C_7H_7)(η-C_5H_5)] but may be hidden by the p → d resonance features.

One of the possible ways of envisaging shape resonances is that the ionizing electron is initially excited to a quasibound antibonding MO, a state which then decays into the molecular ion plus a photoelectron. Good overlap between bound and quasibound MOs is an important factor in the process, and it may well be that the quasibound intermediate MO(s) in these shape resonances are strongly localized in the region occupied by the metal atom. Consequently only MOs with significant metal AO (in the case of the valence MOs, metal d AO) content will experience the shape resonance.

In general, therefore, the cross section results support our previous proposal as to the bonding mode of the cycloheptatrienyl ring to transition metal centers. The principal metal–ligand covalent interaction is in the $1e_2$ MOs, which contain four electrons of mixed metal/ligand character. Three of these electrons can be considered as having come from the metal, and they retain a significant degree of metal d-orbital character in the complex. Hence, if a neutral transition metal possess *n* valence electrons, no more than $(n-3)$ are available for bonding to ancillary ligands in complexes containing the metal and a cycloheptatrienyl ring.

Acknowledgment. The authors wish to thank Dr. Peter Scott and Dr. Sally Jackson for their efforts in synthesizing the molecules described in this study, the machine staff of the Daresbury Laboratory for their efficient running of the Synchrotron Radiation Source, and the Science and Engineering Research Council for financial support.

Supplementary Material Available: Tables listing relative partial photoionization cross sections (4 pages). This material is contained in many libraries on microfiche, immediately follows this article in the microfilm version of the journal, and can be ordered from the ACS; see any current masthead page for ordering information.